Electronic Supplementary Material

Role of oxygen vacancy inducer for graphene in graphene-containing anodes

Fei Wang, Jian Mao (✉)
College of Materials Science and Engineering, Sichuan University, Chengdu 610065, China
E-mail: maojian@scu.edu.cn

Calculation of Li^+ diffusion coefficient based on GITT curves:

$$D = \frac{4}{\pi\tau}\left(\frac{m_B V_M}{M_B S}\right)^2\left(\frac{\triangle E_\tau}{\triangle E_s}\right)^2 \quad \text{(S1)}$$

Where D is diffusion coefficient; m_B and M_B are the active mass and molar mass of the electrodes, respectively; V_M is the molar volume; and S is the total interfacial area between the electrolyte and the electrode.

Calculation of adsorption energy:

The adsorption energy (E_{ad}) is calculated by Eq. S2.

$$E_{ad} = E_{bulk+Li} - E_{bulk} - E_{Li} \quad \text{(S2)}$$

where $E_{bulk+Li}$, E_{bulk} and E_{Li} are the energy of a Li^+ in hosts, hosts and a Li^+.

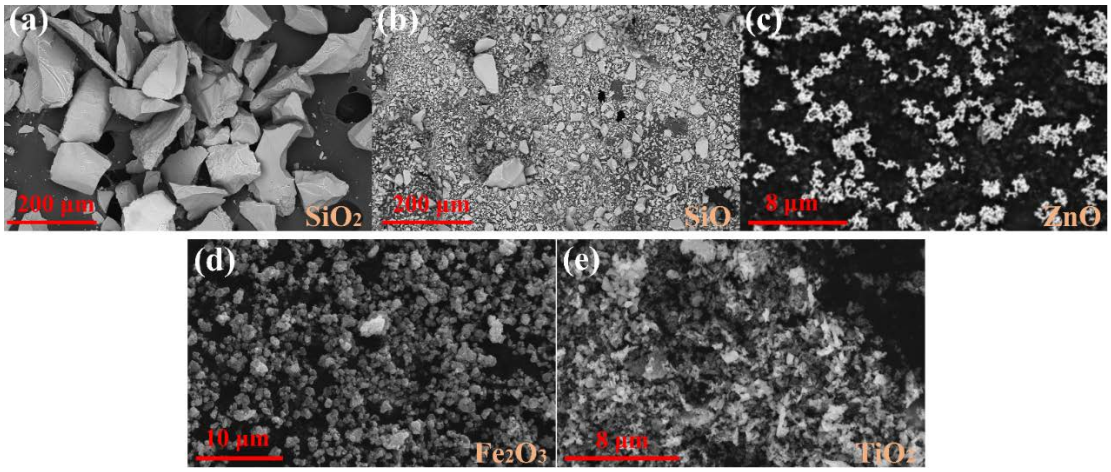

Fig. S1 SEM morphology of **(a)** SiO_2 and **(b)** SiO, **(c)** ZnO, **(d)** Fe_2O_3 and **(e)** TiO_2.

The shape of SiO_2 powder is irregular polyhedron and flake, and the size is about 100-200 μm. The SiO presents irregular polyhedron shape and the size is from nano- to micro-scale. The ZnO is needle-like with the size of about 200 nm. The Fe_2O_3 is sphericity with the size of around 2 μm. The TiO_2 contains nanospheres, nanorods and nano blocks.

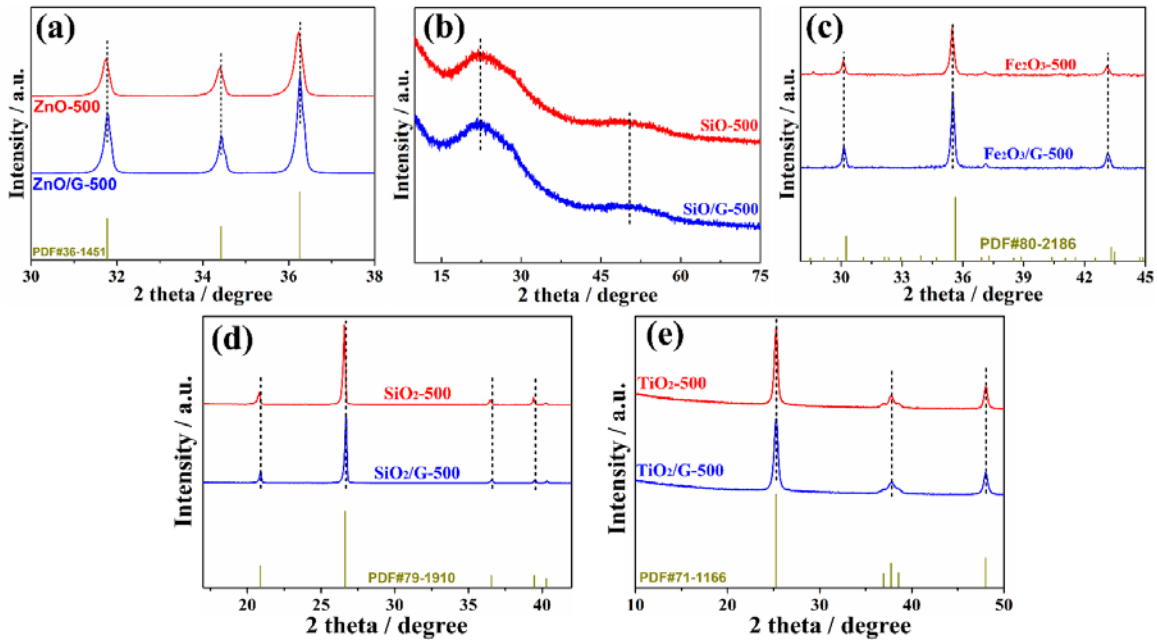

Fig. S2 XRD patterns of **(a)** ZnO-500 and ZnO/G-500, **(b)** SiO-500 and SiO/G-500, **(c)** Fe_2O_3-500 and Fe_2O_3/G-500, **(d)** SiO_2-500 and SiO_2/G-500, and **(e)** TiO_2-500 and TiO_2/G-500.

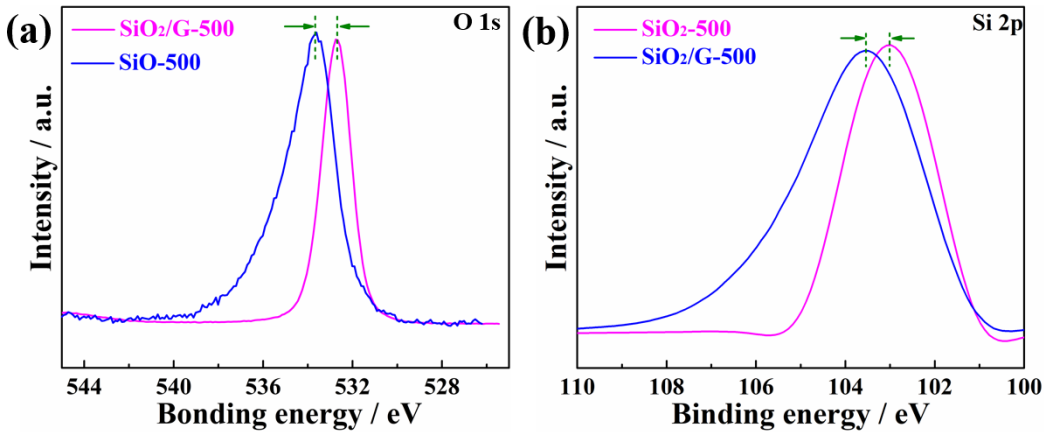

Fig. S3 XPS **(a)** O 1s and **(b)** Si 2p spectra of SiO_2-500 and SiO_2/G-500.

Compared with the SiO_2-500, the O 1s (**Fig. S3(a)**) and Si 2p (**Fig. S3(b)**) spectrum of SiO_2/G-500 shifts to higher energy, indicating that the SiO_2 in SiO_2/G-500 holds a higher concentration of oxygen vacancy. [1]

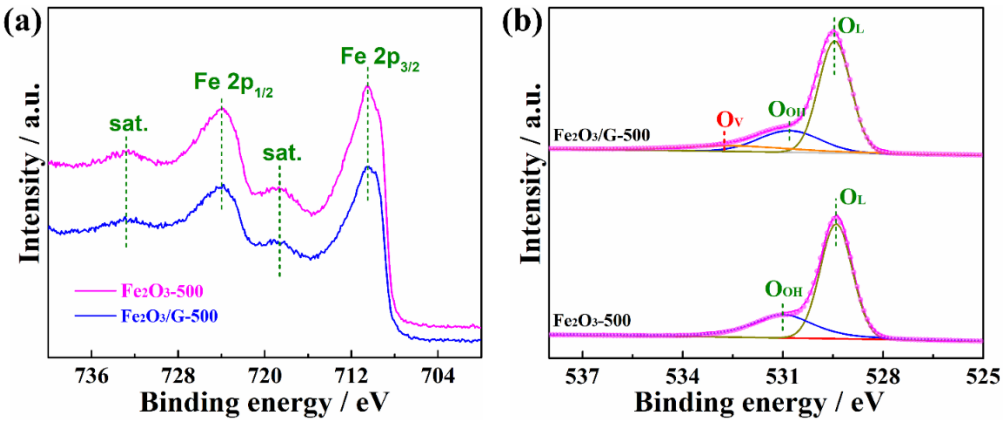

Fig. S4 XPS **(a)** Fe 2p and **(b)** O 1s spectra of Fe_2O_3-500 and Fe_2O_3/G-500.

As shown in **Fig. S4(a)**, the two samples present similar Fe 2p spectra. In **Fig. S4(b)**, the Fe_2O_3-500 only contains lattice oxygen (529.5 eV, O_L) and adsorbed oxygen species (530.8 eV, O_{OH}), while the Fe_2O_3/G-500 has the oxygen vacancy (O_v) peak at 532.8 eV. [2] The results indicate that graphene can facilitate the formation of oxygen vacancies at high temperatures.

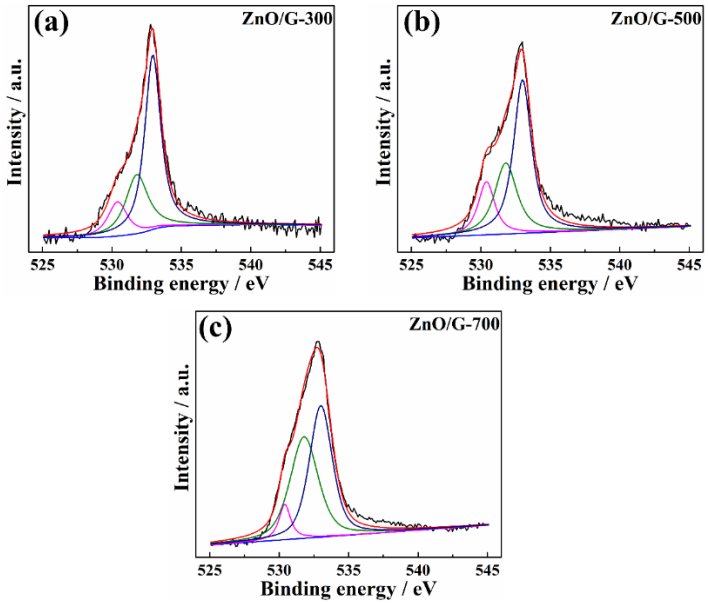

Fig. S5 XPS O 1s spectra of **(a)** ZnO/G-300, **(b)** ZnO/G-500 and **(c)** ZnO/G-700.

The O1s spectra of the three samples can be described as the superposition of three peaks, located at 530.4 eV, 531.8 eV, and 533 eV, respectively. The O1s peak at 533 eV is usually attributed to the presence of adsorbed oxygen species on the surface, the peak at 530.4 eV is attributed to the O^{2-} ions in the lattice, and the peak at 531.8 eV is associated with oxygen vacancy. [3] It is believed that the intensity of this peak is connected to the variations in the concentration of oxygen vacancies. Therefore, the oxygen vacancy concentration gradually increases with the increase of temperature (**Fig. S5**), which is consistent with the EPR analysis.

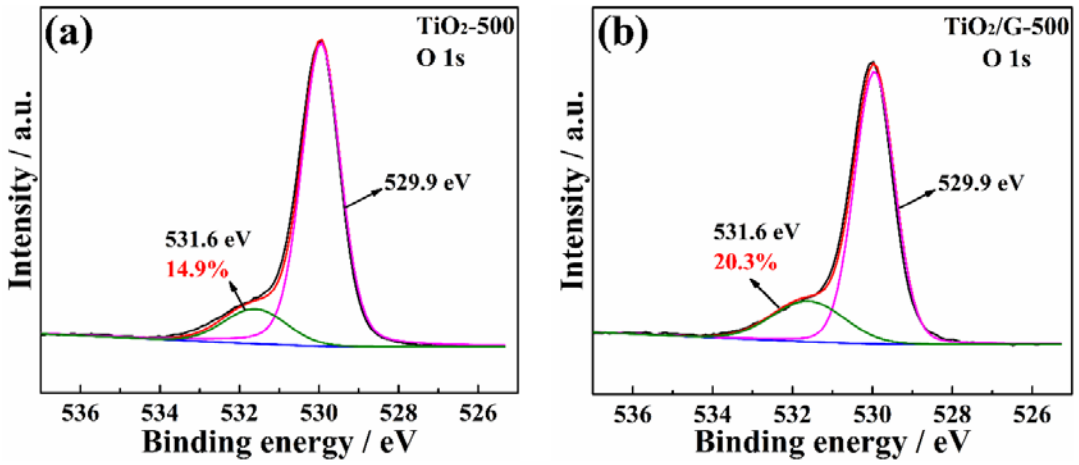

Fig. S6 XPS O 1s spectra of **(a)** TiO_2-500 and **(b)** TiO_2/G-500.

Fig. S6 shows the O 1s XPS spectra of the TiO_2-500 and TiO_2/G-500 samples, which are deconvoluted to two peaks at 529.9 and 531.6 eV, corresponding to the oxygen atoms O^{2-} in the lattice and the absorbed –OH group, respectively. The signal of the absorbed –OH group can represent the existence of oxygen vacancies. [4] The integral area of oxygen vacancies signal in TiO_2/G-500 (20.3%) is higher than that for TiO_2-500, further confirming that the G can induce the formation of oxygen vacancies.

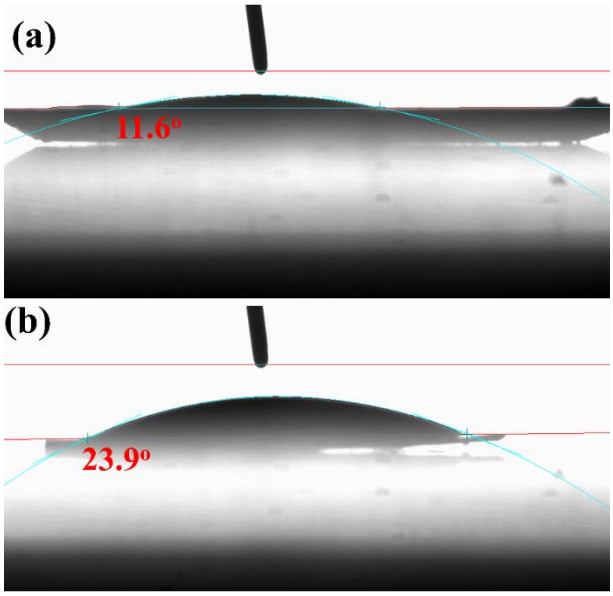

Fig. S7 Contact angles for **(a)** ZnO-500 and **(b)** ZnO.

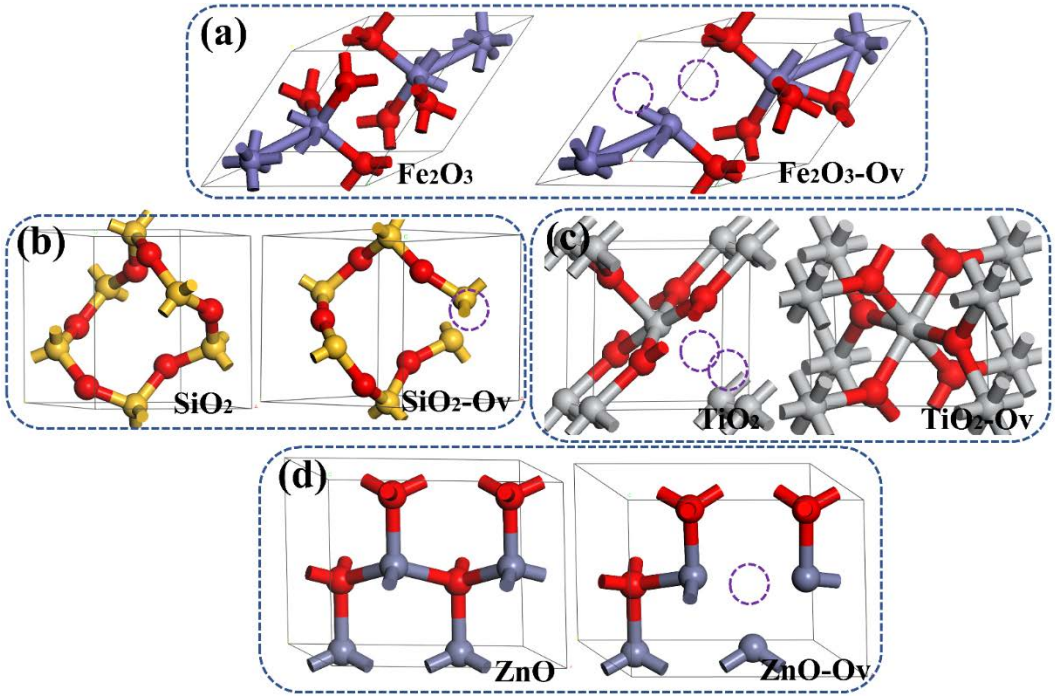

Fig. S8 Models of **(a)** Fe_2O_3 and Fe_2O_3-O_v, **(b)** SiO_2 and SiO_2-O_v, **(c)** TiO_2 and TiO_2-O_v and **(d)** ZnO and ZnO-O_v. The circles denote the oxygen vacancies.

Because the used SiO is an amorphous structure, the SiO is not considered in the DFT simulations.

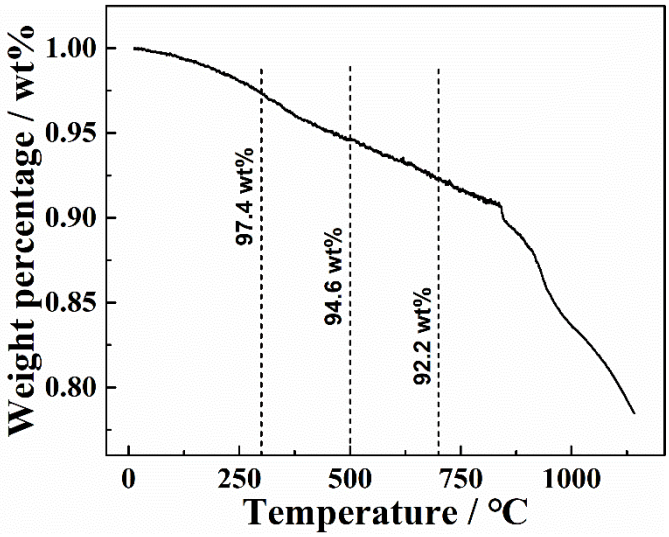

Fig. S9 TG curve of graphene.

When the temperature increases to 300, 500 and 700 ℃, the weight percentage of graphene remains 97.4, 94.6 and 92.2 wt%, respectively.

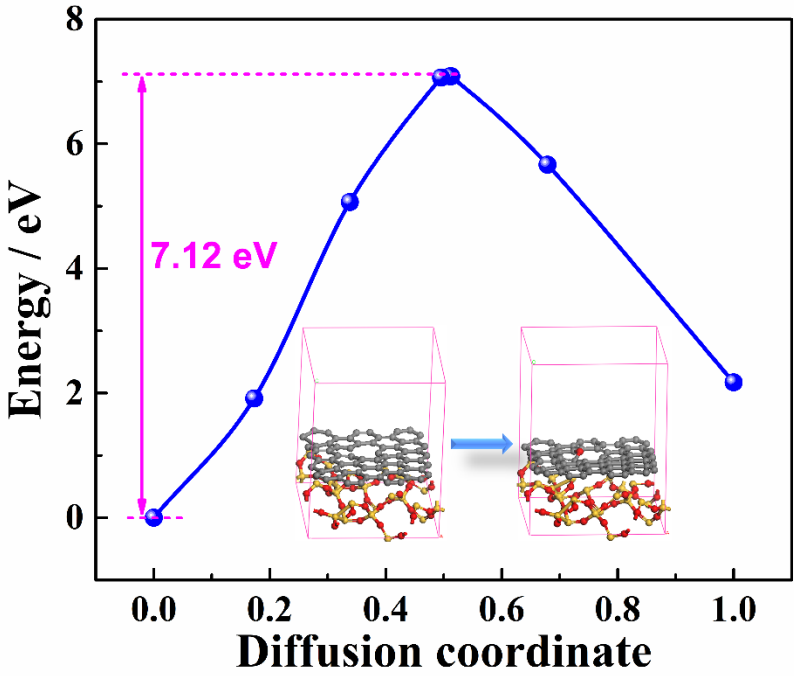

Fig. S10 Energy barriers for formation of an oxygen vacancy in SiO_2 with help of carbon vacancy containing graphene.

For the SiO_2, the energy barrier for the formation of an oxygen vacancy at the surface is 11.14 eV, which has been studied in our previous work.[1] When the graphene with a carbon vacancy is introduced, the energy barrier decreases to 7.12 eV (**Fig. S10**). The result further indicates that graphene can facilitate the formation of oxygen vacancy in oxides.

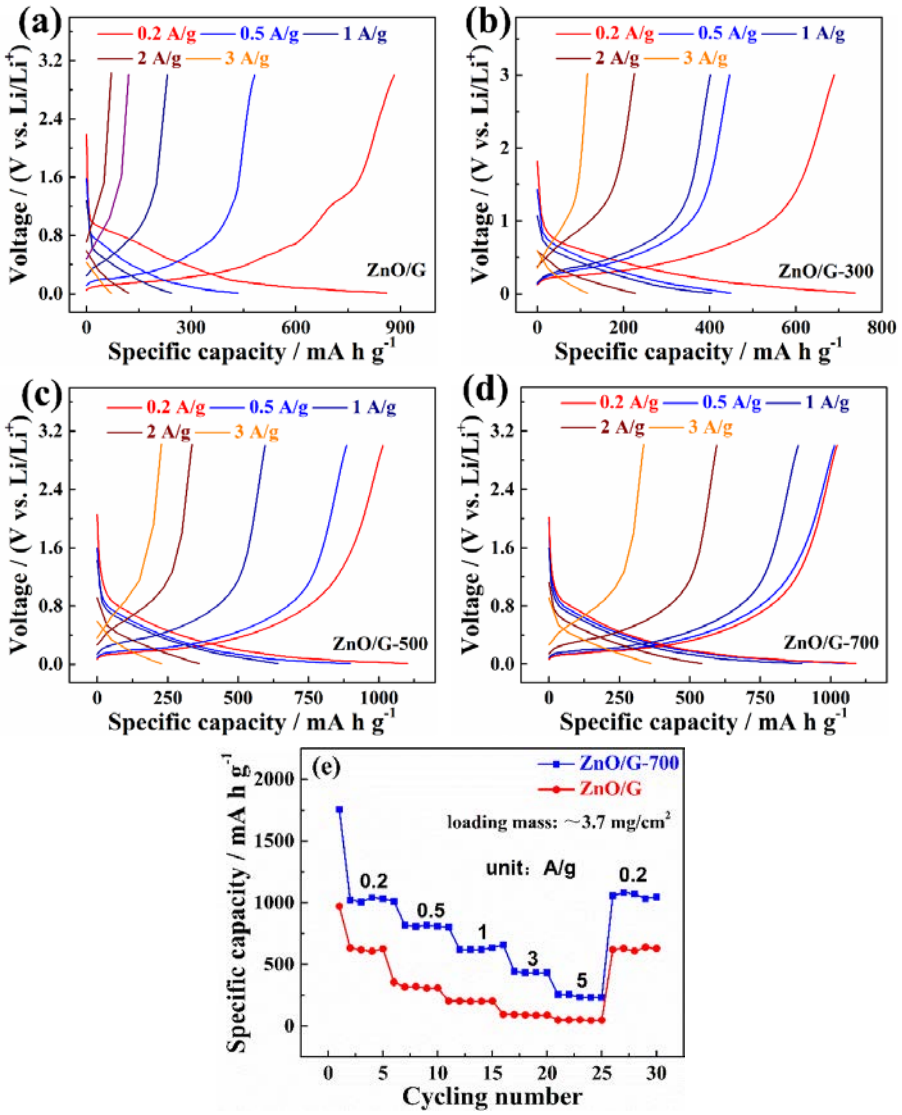

Fig. S11 Voltage-capacity curves of **(a)** ZnO/G, **(b)** ZnO/G-300, **(c)** ZnO/G-500 and **(d)** ZnO/G-700. **(e)** Rate-performace of ZnO/G-700 and ZnO/G with higher loading mass of around 3.7 mg/cm^2.

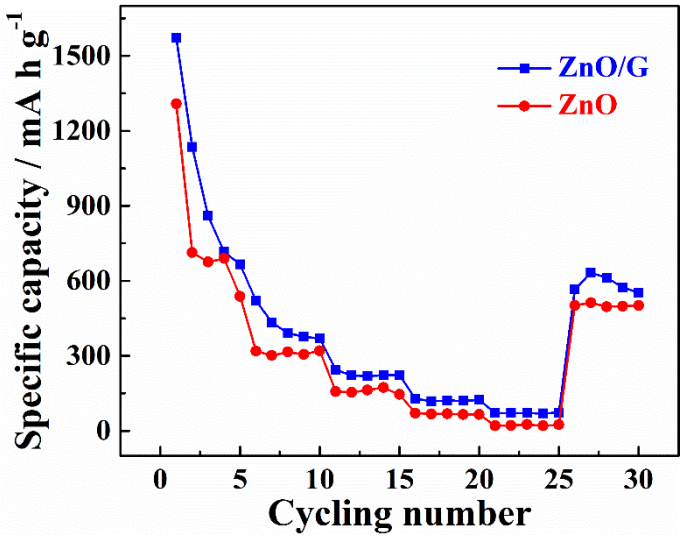

Fig. S12 Rate-performance of ZnO/G and ZnO.

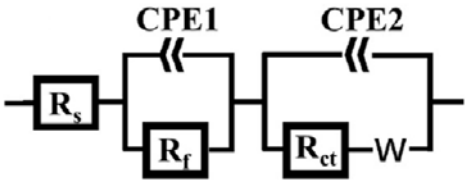

Fig. S13 Used equivalent circuit diagram.

For the equivalent circuit, the R_s, R_f, R_{ct} and W are solution resistance, SEI film resistance, charge transfer resistance and Warburg impedance, respectively. The CPE1 and CPE2 are the constant phase elements of SEI film and electric double layer, respectively.

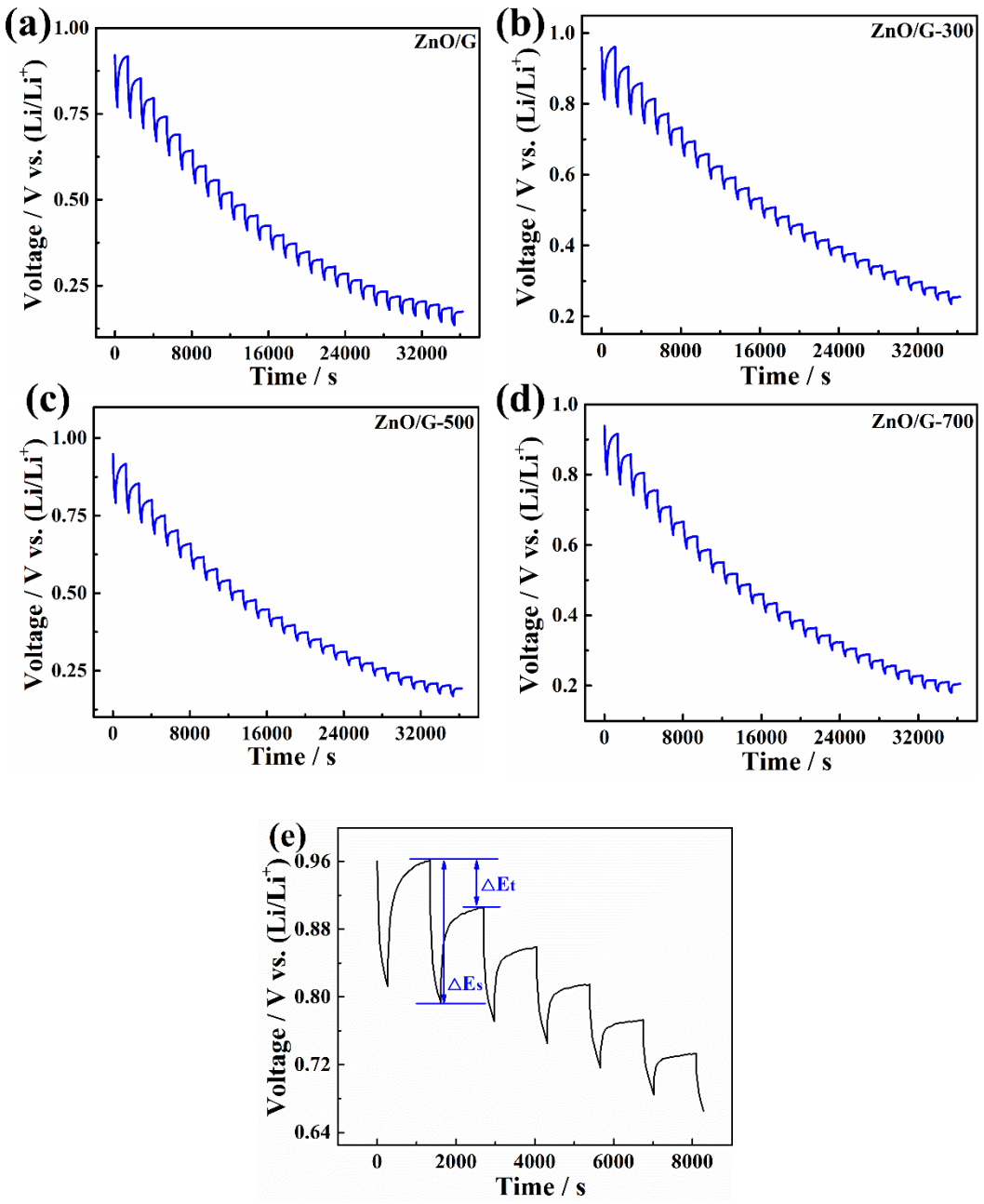

Fig. S14 galvanostatic intermittent titration technique curves curves of **(a)** ZnO/G, **(b)** ZnO/G-300, **(c)** ZnO/G-500 and **(d)** ZnO/G-700. **(e)** Calculation of $\triangle E_t$ and $\triangle E_s$.

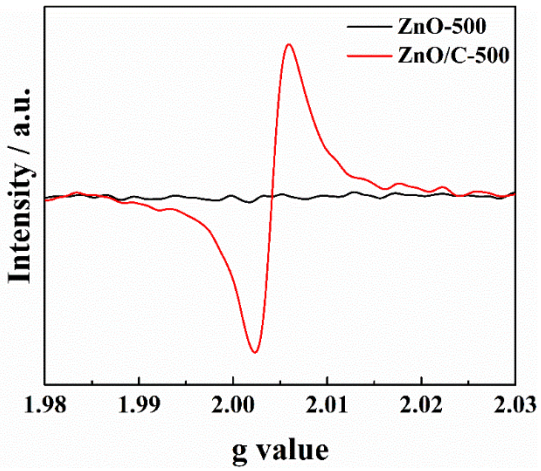

Fig. S15 EPR spectra of **(a)** ZnO-500 and ZnO/C-500.

Tab. S1 R_s and R_{ct} values of ZnO/G, ZnO/G-300, ZnO/G-500 and ZnO/G-700.

Sample	R_s / Ω	R_{ct} / Ω
ZnO/G	2.48	15.78
ZnO/G-300	2.47	9.59
ZnO/G-500	2.01	8.95
ZnO/G-700	2.45	5.45

References

[1] Wang F, Mao L, Qi X, et al. Sulfur-induced abundant oxygen vacancies in hollow silica microsphere toward super anode[J]. Chemical Engineering Journal, 2021,418:129397.

[2] Cao Z, Jiang Z, Cao L, et al. Lattice expansion and oxygen vacancy of α -Fe2O3 during gas sensing[J]. Talanta, 2021,221:121616.

[3] Wang J, Wang Z, Huang B, et al. Oxygen Vacancy Induced Band-Gap Narrowing and Enhanced Visible Light Photocatalytic Activity of ZnO[J]. ACS Applied Materials & Interfaces, 2012,4(8):4024-4030.

[4] Huang X, Gao X, Xue Q, Wang C, et al. Impact of oxygen vacancies on TiO2 charge carrier transfer for photoelectrochemical water splitting. Dalton Transaction, 2020, 49, 2184.